TOPICAL REVIEW

Mechanisms of the formation of biological signaling profiles

To cite this article: Hamid Teimouri and Anatoly B Kolomeisky 2016 *J. Phys. A: Math. Theor.* **49** 483001

IOP Publishing Journal of Physics A: Mathematical and Theoretical
J. Phys. A: Math. Theor. **49** (2016) 483001 (30pp) doi:10.1088/1751-8113/49/48/483001

Topical Review

Mechanisms of the formation of biological signaling profiles

Hamid Teimouri and Anatoly B Kolomeisky

Department of Chemistry and Center for Theoretical Biological Physics, Rice University, Houston, TX, 77005, USA

E-mail: tolya@rice.edu

Received 22 July 2016, revised 25 September 2016
Accepted for publication 29 September 2016
Published 7 November 2016

Abstract

The formation and growth of multi-cellular organisms and tissues from several genetically identical embryo cells is one of the most fundamental natural phenomena. These processes are stimulated and governed by multiple biological signaling molecules, which are also called morphogens. Embryo cells are able to read and pass genetic information by measuring the non-uniform concentration profiles of signaling molecules. It is widely believed that the establishment of concentration profiles of morphogens, commonly referred as morphogen gradients, is a result of complex biophysical and biochemical processes that might involve diffusion and degradation of locally produced signaling molecules. In this review, we discuss various theoretical aspects of the mechanisms for morphogen gradient formation, including stationary and transient dynamics, the effect of source delocalization, diffusion, different degradation mechanisms, and the role of spatial dimensions. Theoretical predictions are compared with experimental observations. In addition, we analyze the potential alternative mechanisms of the delivery of biological signals in embryo cells and tissues. Current challenges in understanding the mechanisms of morphogen gradients and future directions are also discussed.

Keywords: morphogen gradient, biological signaling, reaction–diffusion processes

(Some figures may appear in colour only in the online journal)

1. Introduction

The development of various living organisms from an initially very small group of identical embryo cells is one of the most fascinating and complex processes in biology [1–4]. A critical stage in biological development is a pattern formation during which the eventual fate of cells

becomes determined at different times and different spatial positions. Several classes of biological signaling molecules, known as morphogens, play a central role in the tissue patterning and organ formation in all living systems [1–5]. The term 'morphogen' was first introduced by Turing in his seminal paper on the mathematical modeling of biological pattern formation [6]. In this pioneering work, Turing demonstrated that diffusion and chemical reactions involving several species can produce spatial patterns in an array of cells, which are very similar to patterns observed in nature. Recent experiments have provided a direct verification for Turing's theory in artificial chemical systems [61]. The next critical step was made by Wolpert, who introduced the idea of positional information [4, 13]. He argued that the developmental pattern formation is a result of the interpretation of spatial positions decoded in external signals from biological signaling molecules. Cells obtain the spatial information by somehow 'measuring' the concentration of morphogens around them. Different genes are turned on or off depending on several concentration thresholds, eventually producing morphologically different cells. Finally, Crick realized that dynamic aspects of the creation of morphogen profiles are also important for the proper development of tissues and organs [5]. He emphasized the important role of diffusion because of a limited time window for development processes. These three fundamental concepts are the foundations of the modern theory of morphogen gradients [7–10, 12].

Enlightened by these ideas, a large number of experiments on the formation, regulation and functioning of morphogen gradients has appeared in recent years. They clearly show that the non-uniform concentration profiles of signaling molecules are responsible for symmetry breaking, tissue development and organ formation in multi-cellular organisms [7–10, 12, 14–19, 24–27, 29, 33, 41, 46, 83]. Although these investigations of morphogen gradients were done on diverse biological systems, most studies focused on two main examples. The first one is a Drosophila embryo where Bicoid (Bcd) morphogen gradients and the corresponding patterns were monitored and analyzed [7–9, 16, 27, 33, 46]. The second example is a pattern formation in vertebrate neural tubes by Sonic hedgehog morphogens [8, 20, 48, 49]. A large amount of quantitative information has been assembled on these systems which highlight the importance of morphogen gradients. Another striking observation is that, despite different evolutionary origins, distinct cell biology and biochemistry, the formation of tissue patterns is very similar in both organisms [8].

The analysis of developmental processes in different systems suggested the existence of several universal mechanisms governing the establishment of signaling profiles and their activities [7–9, 12]. Stimulated by these experimental observations, a large number of theoretical ideas on the mechanisms of the formation of morphogen gradients have been proposed [7–10, 12, 21, 21–23, 28, 31, 32, 34–40, 43, 50, 51, 58, 59, 76–78, 80]. Most of these studies suggest that the establishment of biological signaling profiles in development is a result of complex physical–chemical processes that include the localized production of morphogens that can later diffuse and be removed from the cellular medium by various types of biochemical transitions [7–10, 12]. Based on some experimental observations [64, 65, 67, 68, 70, 71, 74], the possibility of alternative mechanisms of the direct delivery of morphogens to the target cells utilizing dynamic cellular extensions called cytonemes was predicted [11, 64, 77]. It has been argued that the complex environment of the embryo systems might prevent the free diffusion from establishing the distinguishable morphogen gradients at different regions, implying a different mechanism of the biological signal transduction [11, 64].

In this paper, a brief overview of the mechanisms of the development of morphogen gradients is presented. Because of the large number of excellent reviews on morphogens [7–10, 12], we concentrate here only on the theoretical aspects of the formation of biological

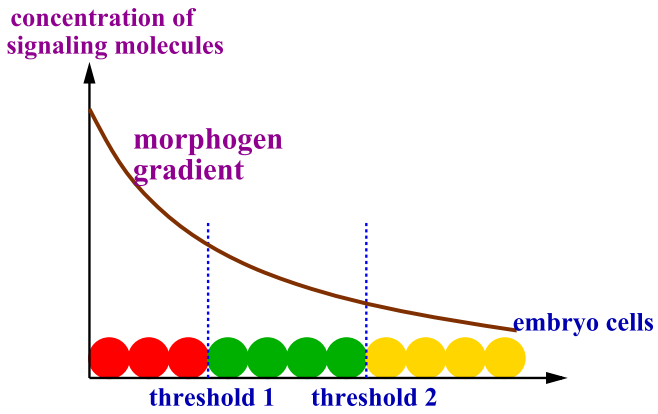

Figure 1. A schematic view of the morphogen gradient and its action on embryo cells. Cells exposed to the morphogen concentration above threshold 1 will activate a 'red' gene; cells exposed to the morphogen concentration below threshold 1 but above threshold 2 will activate a 'green' gene; and cells exposed to the morphogen concentration below threshold 2 will activate a 'yellow' gene.

signaling profiles. For this reason, the important subjects, such as how cells interpretate the graded signals and biochemical regulations of these signals, are not discussed [12, 47]. Furthermore, in analyzing the complex processes associated with the establishment of morphogen gradients, we benefited from multiple discussions with many researchers. But this review presents our subjective view on the field, which might disagree with some existing descriptions.

2. Development of morphogen gradients via reaction–diffusion processes

Before exploring the mechanisms of the formation of biological signaling profiles, it is important to describe what these signaling molecules are, which are also known as morphogens. They are protein molecules that are responsible for passing on the information in the developing embryos as to where and which tissues should appear [7–10, 12]. The time scales for the pattern formation in biological systems range from 1–2 h in *Drosophila* to 20 h in mammals [8], reflecting the differences in cell biology of underlying organisms.

The dominating view in the field is that the morphogen gradients are created by a complex action of several reaction–diffusion processes [7–10, 12]. Two main theoretical directions have been explored in clarifying the mechanisms of the formation of signaling profiles. One of them utilizes a continuum description, while another one is based on more general discrete-state stochastic analysis of the processes. Below we discuss and compare both of them.

2.1. Continuum synthesis-diffusion-degradation model

Experiments show that biological signaling profiles are not uniform, as shown in figure 1. This lead to the formulation of the simplest, and still the most popular, idea on the formation of morphogen gradients. It is known as a *synthesis-diffusion-degradation* (SDD) model [7–10, 12]. It is the most frequently applied model for analyzing multiple systems where the profiles of signaling molecules are formed [7–10, 12].

To describe this model mathematically, let us consider a semi-infinite signaling domain in which morphogens are produced at the origin, $x = 0$, with a rate Q. They diffuse along the field of cells with a diffusion constant D or they might be degraded with a rate k. One can define a function $C(x, t)$ as the concentration of morphogens at position x at time t. The temporal evolution of the concentration profile follows from a corresponding reaction–diffusion equation,

$$\frac{\partial C(x, t)}{\partial t} = D\frac{\partial^2 C(x, t)}{\partial x^2} - kC(x, t), \tag{1}$$

with the boundary condition at the origin

$$\left.\frac{\partial C(x, t)}{\partial x}\right|_{x=0} = -Q. \tag{2}$$

Assuming that initially there were no morphogens in the system, $C(x, t = 0) = 0$, these equations can be exactly solved at all times, yielding the following concentration profile [23],

$$C(x, t) = C^{(s)}(x)\left[1 - \frac{1}{2}\mathrm{erfc}\left(\frac{\sqrt{Dt}}{\lambda} - \frac{x}{2\sqrt{Dt}}\right) - \frac{1}{2}\mathrm{e}^{-2x/\lambda}\mathrm{erfc}\left(\frac{\sqrt{Dt}}{\lambda} + \frac{x}{2\sqrt{Dt}}\right)\right], \tag{3}$$

where $\mathrm{erfc}(y)$ is the complementary error function, $\lambda = \sqrt{D/k}$, and $C^{(s)}(x)$ is the stationary profile,

$$C^{(s)}(x) = \frac{Q}{\sqrt{Dk}}\exp\left(-\frac{x}{\lambda}\right). \tag{4}$$

The SDD model predicts that at large times ($t \to \infty$) the morphogen gradient is the exponentially decaying function of the distance from the source with a length scale λ determined by the ratio of the diffusion and degradation rates. These predictions qualitatively agree with many observations of morphogen gradients in various systems [16, 19, 24, 27, 46]. However, the application of this model for more quantitative measurements of the dynamics of the formation of signaling profiles in Bcd led to some controversial results [16]. Experiments suggested that Bcd molecules diffuse relatively slowly with $D \simeq 0.3\ \mu\mathrm{m}^2\ \mathrm{s}^{-1}$ [16]. The most distant location that is still affected by the Bcd molecules is at $L \simeq 375\ \mu\mathrm{m}$ [34]. Using the unbiased random walk arguments, one can evaluate how long it takes for the morphogens to diffuse to this location, $\tau = L^2/2D \simeq 4000$ min, providing the estimate for the formation of the Bcd profile in *Drosophila* embryos. But this contradicts the experimental observation that the morphogen gradient is created in approximately 90 min in the whole embryo system. Clearly, there is a discrepancy between these theoretical predictions and what is measured directly in experiments [16]. Several early attempts to explain this controversy turned out to be unsuccessful [79].

Progress in resolving this paradox of slow diffusion and fast formation of the morphogen gradients has been achieved by Berezhkovskii and coworkers who introduced a new method of analyzing the dynamics [21, 34–36, 43]. They realized that the correct estimate of the times to establish the morphogen gradient is given by the relaxation times to reach the stationary-state profiles, which are labeled as *local accumulation times* (LAT) [34–36]. To obtain LAT, one has to first define local relaxation functions,

$$R(x, t) = \frac{C(x, t) - C^{(s)}(x)}{C(x, t = 0) - C^{(s)}(x)} = 1 - \frac{C(x, t)}{C^{(s)}(x)}. \tag{5}$$

The physical meaning of these functions is that they represent a relative distance to the stationary state: at $t = 0$ the distance is one, while at the steady state it is equal to zero. The

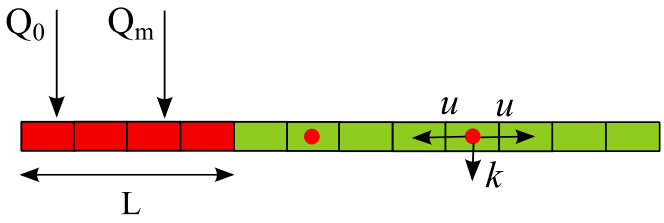

Figure 2. A schematic view of the one-dimensional discrete-state SDD model for the formation of the morphogen gradients. The production of morphogens is distributed over an interval of length L. Signaling molecules are produced at the sites $0 \leqslant m \leqslant L$ (shown in red) with rates Q_m. The case of $m = 0$ and $L = 1$ corresponds to the source localized at the origin. Particles can also diffuse along the lattice to the neighboring sites with a rate u, or they might be degraded with a rate k. Adapted with permission from [75], copyright 2015 IOP Publishing.

function $\left(-\frac{\partial R(x,t)}{\partial t}\right)$ is the probability density for reaching the stationary state at the position x at time t. The explicit formulas for the local accumulation time can be derived then via Laplace transformations of the local relaxation function, $\widetilde{R}(x, s) = \int_0^\infty R(x, t)\mathrm{e}^{-st}\mathrm{d}t$ [34],

$$t(x) = \int_0^\infty t\left(-\frac{\partial R(x, t)}{\partial t}\right)\mathrm{d}t = \widetilde{R}(x, s = 0). \tag{6}$$

For the SDD model, from equations (3) and (5) it can be shown that the relaxation function is given by

$$R(x, t) = \mathrm{erfc}\left(\frac{\sqrt{Dt}}{\lambda} - \frac{x}{2\sqrt{Dt}}\right) + \frac{1}{2}\mathrm{e}^{-2x/\lambda}\mathrm{erfc}\left(\frac{\sqrt{Dt}}{\lambda} + \frac{x}{2\sqrt{Dt}}\right), \tag{7}$$

which leads to a very simple expression for the LAT [34],

$$t(x) = \frac{1}{2k}\left(1 + \frac{x}{\lambda}\right). \tag{8}$$

For the Bcd morphogen gradient, using expression (8) along with the estimate of the decay length $\lambda \simeq 60$ μm and with a better estimation of the diffusion constant $D \simeq 1$ $\mu\mathrm{m}^2$ s^{-1} [22, 53], the time to reach the stationary state at the most distant boundary was calculated to be less than 200 min, which is much closer (although still not perfect) to the experimental values ($\simeq$90 min). The difference between these theoretical predictions and experiments is probably due to the imprecise measurements of the diffusion constant and the decay length, as well as due to the oversimplified theoretical assumptions of the strongly localized source region, as we discuss below in more detail [34]. Thus, the systematic approach to evaluate LAT as a measure of the dynamics of the formation of morphogen gradients was able to mostly resolve the paradox of slow diffusion [34]. However, it also raised several fundamental questions. Equation (8) indicates a linear scaling as the distance from the source for the SDD model instead of the expected quadratic scaling for the unbiased random walk motion since there are no apparent external driving forces in the system. It led to a conclusion that signaling profiles formed much faster than was previously estimated [34, 45, 57]. But the mechanism of this acceleration was not clear.

2.2. Discrete-state stochastic description

During the establishment of the signaling profile, the morphogen molecules are removed from the medium at specific locations of the cells (usually at receptors), and this implies that the overall process is intrinsically biochemically discreet. This suggests that the continuum description of the formation of morphogen gradients is an approximation, and it might not fully describe these processes at all conditions [57]. For this reason, a more general discrete-state stochastic framework was introduced [57].

The discrete version of the SDD model is presented in figure 2. It is assumed that each embryo cell is associated with a lattice site. In the simplest version of the model, the morphogens are produced only at the origin with a rate $Q_0 = Q$ ($L = 1$ case in figure 2). Signaling molecules can diffuse with a rate u along the lattice. At any position, the morphogen can be degraded and removed from the system with a rate k. The continuum description is obtained in the limit of very fast diffusion, $u \gg k$. To simplify the calculations, a single-molecule view, according to which the concentration of morphogens at a given site is equivalent to the probability of finding the signaling molecule at this location, was adopted [57]. A function $P_n(t)$, defined as the probability of finding the morphogen at site n at time t, was introduced [57]. The temporal evolution of this probability is governed by the following master equations,

$$\frac{\mathrm{d}P_0(t)}{\mathrm{d}t} = Q + uP_1(t) - (u + k)P_0(t) \tag{9}$$

for $n = 0$; and

$$\frac{\mathrm{d}P_n(t)}{\mathrm{d}t} = u[P_{n-1}(t) + P_{n+1}(t)] - (2u + k)P_n(t) \tag{10}$$

for $n > 0$. At large times, where $\frac{\mathrm{d}P_n(t)}{\mathrm{d}t} = 0$, these equations can be easily solved, producing the exponentially decaying profile,

$$P_n^{(s)} = \frac{2Qx^n}{k + \sqrt{k^2 + 4uk}} \tag{11}$$

with

$$x = (2u + k - \sqrt{k^2 + 4uk})/(2u). \tag{12}$$

In the continuum limit, $u \gg k$, equation (11) reduces, as expected, to expression (4). The characteristic length of the concentration decay is given by

$$\lambda = -\frac{1}{\ln x}. \tag{13}$$

In the case of fast diffusion rates, $u \gg k$, this length is equal to $\lambda \simeq \sqrt{u/k}$ which is a well-known result for the continuum SDD model [34]. In another limit of fast degradation rates, $k \gg u$, this length is very small $\lambda \simeq \frac{1}{\ln(k/u)}$ because the morphogen molecules cannot move large distances from the source due to fast degradations [57].

Calculating LAT for the discrete-state version of the SDD model, the linear scaling was found again [57],

$$t_n = \frac{1}{\sqrt{k^2 + 4uk}}\left[\frac{2u + k + \sqrt{k^2 + 4uk}}{k + \sqrt{k^2 + 4uk}} + n\right]. \tag{14}$$

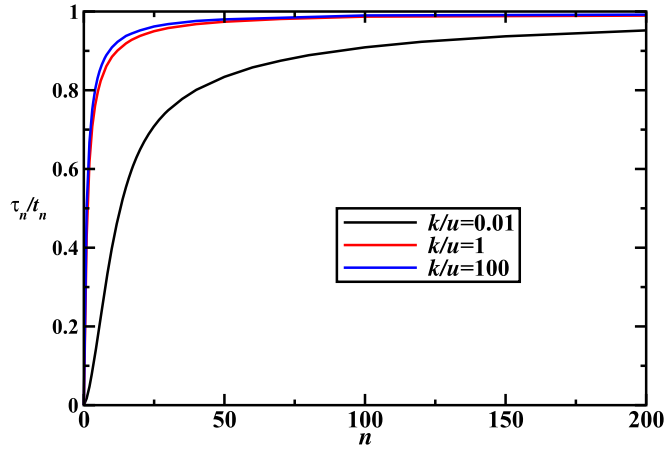

Figure 3. Ratio of LAT and MFPT for the one-dimensional discrete-state stochastic SDD model as a function of the distance from the source for different diffusion and degradation rates. Reprinted with permission from [57]. Copyright 2011 American Chemical Society.

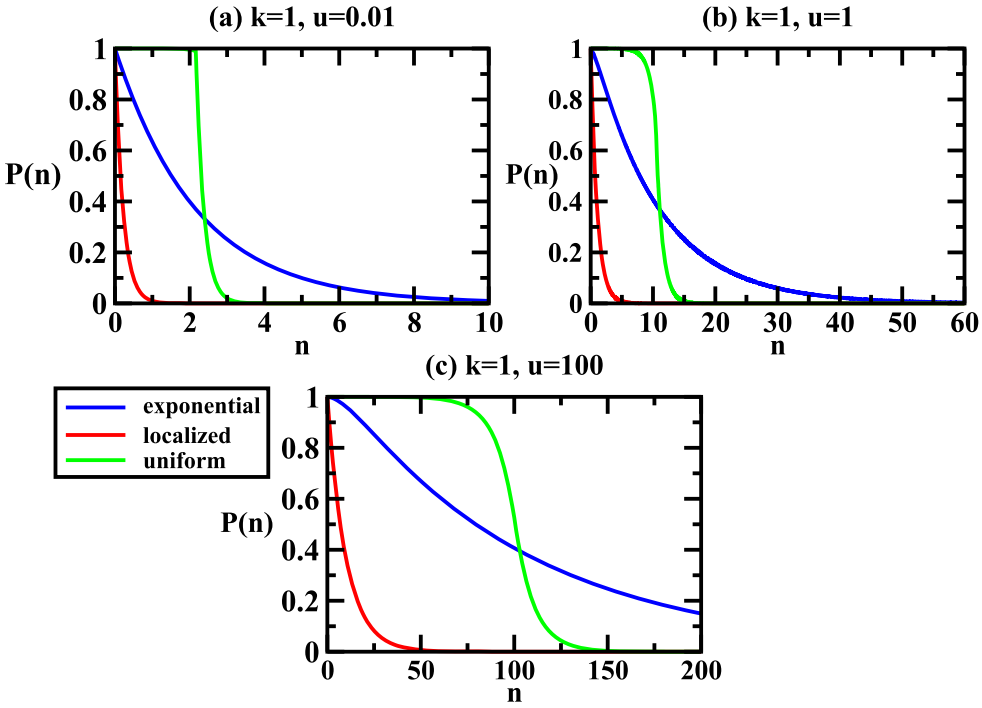

Figure 4. Stationary-state density profiles for the formation of morphogen gradients with different production regions and for variable diffusion and degradation rates. The red curves describe the single-site localized source, the green curves describe the uniform production over the finite interval, and the blue curves describe the exponential production over the semi-infinite interval. Adapted with permission from [75], copyright 2015 IOP Publishing.

In the limit of fast diffusion rates, which describes the continuum regime, this expression reduces to equation (8), while at another limit of fast degradation rates, it produces $t_n \simeq (n+1)/k$. But for all regimes, a linear scaling as a function of the cell position n is again observed, implying a faster than expected formation of the morphogen gradient.

To explain such fast relaxation to the stationary-state profiles, the following arguments were presented [57]. Initially, at $t = 0$, the morphogen molecules start at the origin ($n = 0$), and there is nothing at the site $n > 0$. Then the relaxation time to reach the stationary-state at site n should consist of two contributions. The first one comes from the fact that the signaling molecules first have to reach site n, and it can be associated with a mean first-passage time (MFPT) to arrive here. It is expected that MFPT should strongly depend on n. The second contribution is due to local fluctuations at the given site until the stationary-state conditions are reached. It was argued that this term, labeled as a *local rearrangement time*, is weakly dependent on the position along the lattice. Thus, at large distances from the origin ($n \gg 1$) the local relaxation time can be well approximated by the MFPT, which can be calculated exactly using the backward-master equations [57, 81, 82]. These arguments are illustrated in figure 3 where the ratios of LAT to MFPT are plotted as a function of the distance from the source. In all cases, both time scales approach each other at large n. Later, these theoretical predictions were explicitly proven by Berezhkovskii and Shvartsman [35], who also showed that the local rearrangement time can be viewed as the LAT if the source is localized at the observation point.

But the fact that the LAT can be well approximated by the first arrival time is not enough to explain the fast relaxation to the stationary-state profiles. It was argued that the critical part of the process is the particle removal from the medium [57]. Morphogen molecules have a nonzero probability of being removed from the system at each site due to degradation. To survive on the lattice, the morphogen molecules must move faster or they will be removed. This corresponds to an effective speeding-up of the surviving signaling molecules. It can be also viewed as a fact that the degradation creates an effective potential $U_{\rm eff}(n)$ that drives the morphogens along the lattice away from the source. This potential can be estimated from the stationary-state profile [57],

$$U_{\rm eff} \simeq k_{\rm B}T \ln P_n^{(s)}. \tag{15}$$

For the discrete-state SDD model, this leads to the strongly decreasing linear potential, $U_{\rm eff} \simeq n \ln x = -n/\lambda$, which implies that there is a constant effective force,

$$F_{\rm eff} = -\frac{\partial U_{\rm eff}(n)}{\partial n} = \frac{1}{\lambda}, \tag{16}$$

which drives the morphogens away from the origin. However, the most important conclusion from these arguments is that the motion of the signaling molecules in such a potential is a driven process. It is not the unbiased diffusion as was earlier assumed. This should naturally lead to the linear scaling in time [57]. It is important to note that each molecule has no bias in its motion, but because the concentration due to the degradation decreases for larger n the overall flux in the system will flow in the direction of larger n. This is similar to the effect of the constant force acting in the positive direction. These theoretical arguments provide a microscopic explanation for the fast formation of morphogen gradients, and they also emphasize the critical role of the degradation processes [57].

2.3. The effect of source delocalization

Although the simplest SDD model was able to explain some aspects of the development of morphogen gradients, it was pointed out that many realistic features of the process that might strongly influence the dynamics are not taken into account [30, 31, 34–37, 57, 75]. Experiments show that in many biological systems, the production region of the signaling molecules is not strongly localized as assumed in the simplest SDD model [7–10, 12, 30]. Morphogens are protein molecules that must be first synthesized from the corresponding RNA molecules, but the distributions of RNA species in various embryos are more diffuse [42]. For example, for the Bcd system, it is known that the maternal RNA molecules can be found in the region of size 30–50 μm, which should be compared with the total length of the embryo of $\simeq$400 μm [7].

To understand the role of the spatial delocalization of the production region, several theoretical investigations have been performed [31, 37, 75]. The formal general solution to describe the formation of morphogen gradients from an arbitrary source (as presented in figure 2) has been obtained using the Green's function method in the continuum approximation [31, 37]. In this case, the corresponding reaction–diffusion equation can be written as

$$\frac{\partial C(x,\,t)}{\partial t} = D\frac{\partial^2 C(x,\,t)}{\partial x^2} - kC(x,\,t) + S(x,\,t), \tag{17}$$

where $S(x,\,t)$ is a function that describes the maternal RNA distribution. It was shown that the time-dependent solution of this equation is given by [31, 37],

$$C(x,\,t) = \int \mathrm{d}s \int \mathrm{d}y G(x-y,\,t-s)S(y,\,s), \tag{18}$$

where $G(x,\,t)$ is the Green's function for this system,

$$G(x,\,t) = \frac{1}{\sqrt{4\pi Dt}}\exp\left(-\frac{x^2}{4Dt}\right)\exp(-kt). \tag{19}$$

The physical meaning of this function is the probability of finding the particle at position x at time t if it started from the origin at $t = 0$ [37].

Using this approach, the problems of the formation of morphogen gradients with the source production uniformly distributed over the interval have been analyzed [31, 37]. It was found that the stationary-state profile is flattening near the origin, in agreement with observations for Bcd signaling profiles. In addition, it was argued that the almost constant profile at the beginning of the embryo region explains why the target genes are never expressed close to the origin; a sharper gradient is needed in order to reliably turn off genes at the specific locations [31, 37]. Furthermore, using this method, more complex normal distribution of production over the whole embryo length, as well as time-dependent source productions, were investigated. A similar analysis, which emphasized more the diffusion of RNA in the establishment of the signaling profiles, has been done in [62]. The dynamics of the development of morphogen gradients in the continuum approximation was evaluated using LAT [37]. Specifically, the case of the exponentially distributed source over the semi-infinite interval, i.e. for $L \to \infty$ in figure 2, with the productions rates

$$S(x) = \frac{Q}{\lambda_s}\exp\left(-\frac{x}{\lambda_s}\right) \tag{20}$$

was studied. Here, λ_s is the average decay length for the exponential distribution. It was shown that for this system LAT is equal to [37]

$$\tau_L(x,\,\lambda_s) = \frac{1}{2k}\left[\left(1+\frac{x}{\lambda}\right)\frac{\lambda e^{-x/\lambda}}{\lambda e^{-x/\lambda} - \lambda_s e^{-x/\lambda_s}} + \frac{2\lambda_s^2}{\lambda_s^2 - \lambda^2}\right]. \tag{21}$$

For the case of $\lambda_s = \lambda$ this equation simplifies into

$$\tau_L(x,\,\lambda_s = \lambda) = \frac{1}{4k}\left[3 + \frac{x^2}{\lambda(x+\lambda)}\right]. \tag{22}$$

This expression can be used to estimate the times to create Bcd morphogen gradients. Using $\lambda \simeq 60$ μm, $x \simeq 6\lambda$, and $D \simeq 1$ μm^2 s^{-1}, one can obtain that $\tau \simeq 120$ min, which is very close to the experimentally observed 90 min [16]. These calculations suggest that the extended source accelerates the dynamics of the development of signaling profiles.

A more general theoretical method to evaluate the role of the source delocalization was introduced later [75]. A discrete-state stochastic SDD model in one dimension with the extended source range, as illustrated in figure 2, was considered. It was assumed that the signaling molecules are produced over the interval of length L with rates Q_m for $0 \leqslant m \leqslant L$: see figure 2. The total production rates is equal to $Q = \sum_{m=0}^{L} Q_m$. Because the production of morphogens at different sites is independent from each other, it was suggested that the general solution for the probability of finding a signaling molecule at site n at time t with a delocalized production region as specified in figure 2, $P(n,\,t)$, can be written as a sum of the probabilities $P(n,\,t;\,m)$ for the single localized sources at sites m [75]. More specifically, the probability function $P(n,\,t;\,m)$ is governed by the following master equations,

$$\frac{dP(n,\,t;\,m)}{dt} = Q_m\delta_{m,n} + u[P(n-1,\,t;\,m) + P(n+1,\,t;\,m)] - (2u+k)P(n,\,t;\,m) \tag{23}$$

for $n > 0$, and

$$\frac{dP(0,\,t;\,m)}{dt} = Q_0\delta_{m,0} + uP(1,\,t;\,m) - (u+k)P(0,\,t;\,m) \tag{24}$$

for $n = 0$. In the steady-state limit, $t \to \infty$, these equations can be solved explicitly, yielding

$$P_1^{(s)}(n;\,m) = \frac{Q_m[(k+\sqrt{k^2+4uk})x^{m-n} + (-k+\sqrt{k^2+4uk})x^{n+m})]}{(k+\sqrt{k^2+4uk})\sqrt{k^2+4uk}} \tag{25}$$

for $0 \leqslant n \leqslant m$, and

$$P_2^{(s)}(n;\,m) = \frac{Q_m[(k+\sqrt{k^2+4uk})x^{n-m} + (-k+\sqrt{k^2+4uk})x^{n+m})]}{(k+\sqrt{k^2+4uk})\sqrt{k^2+4uk}} \tag{26}$$

for $m \leqslant n$. The parameter x is given in equation (12). Then using the superposition arguments, it can be shown that

$$P(n,\,t) = \begin{cases} \sum_{m=0}^{n} P_2(n,\,t;\,m) + \sum_{m=n+1}^{L} P_1(n,\,t;\,m), & \text{for } 0 \leqslant n \leqslant L; \\ \sum_{m=0}^{L} P_2(n,\,t;\,m), & \text{for } L \leqslant n. \end{cases} \tag{27}$$

This method allowed us to analyze the formation of morphogen gradients for an arbitrary length of the production region and for arbitrary production rates [75]. In addition, it also leads to the computation of the dynamic properties for the development of the signaling profiles by evaluating the relaxation to the stationary-state profiles [75]. To clarify the role of

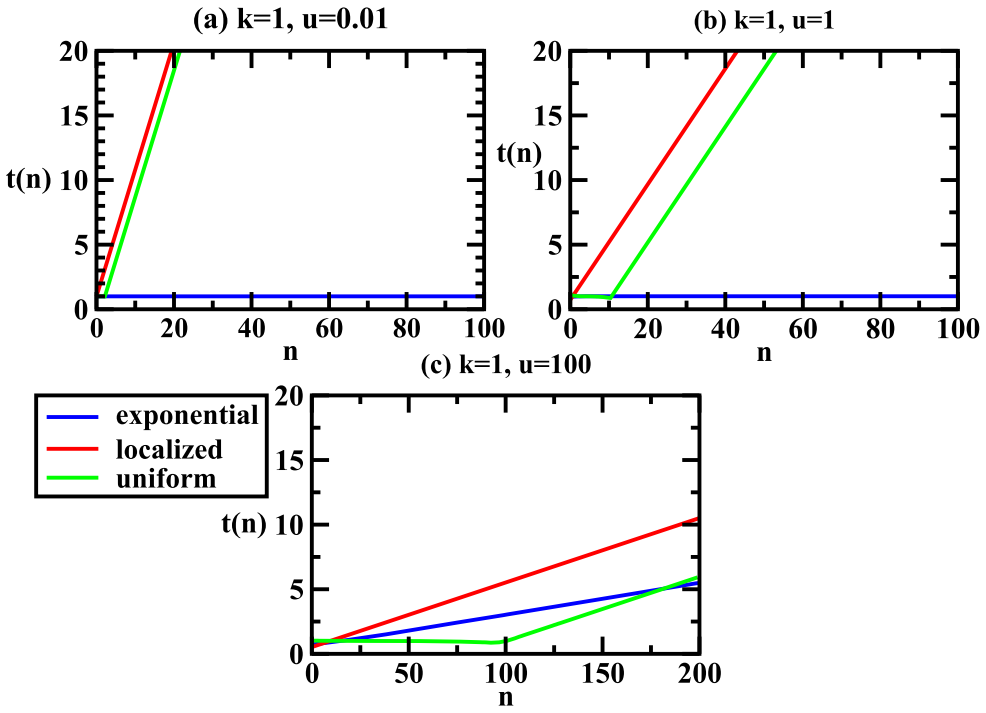

Figure 5. Local accumulation times for the formation of morphogen gradients with different production regions and for variable diffusion and degradation rates. The red curves describe the single-site localized source, the green curves describe the uniform production over the finite interval, and the blue curves describe the exponential production over the semi-infinite interval. Adapted with permission from [75], copyright 2015 IOP Publishing.

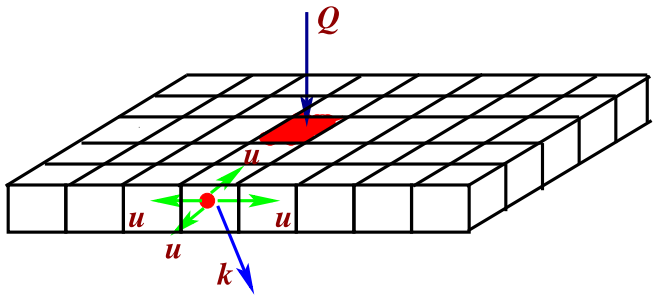

Figure 6. A schematic view of the multi-dimensional system with the formation of morphogen gradients for $d = 2$. The signaling molecules are created at the origin with rate Q. They diffuse with rate u in all directions without a bias. At each cell, morphogens can be degraded with rate k. Adapted with permission from [60], copyright 2014 AIP Publishing LLC.

the source delocalization, the development of the morphogen gradients with uniform distributed production over the finite interval, and with the exponentially distributed production along the semi-infinite interval, were compared with the formation of the signaling profile in

the case of the sharply localized source at the origin [75]. The corresponding density profiles are presented in figure 4, while the estimated LAT are given in figure 5. It was concluded that the extended sources delivered the signaling molecules much further in comparison with the single localized source. In addition, the delocalized sources were able to create sharp boundaries which are needed to controllably turn genes on. They were also generally faster in reaching the stationary states.

2.4. The formation of morphogen gradients in two and three dimensions

Most of the theoretical models applied to describe the establishment of the biological signaling profiles are essentially one-dimensional [34–37, 57, 75]. However, a more realistic description of these processes should take into account a complex structure of the embryos [22, 52]. This has led to multi-dimensional generalizations of the original SDD models [43, 44, 60].

First, continuum radially symmetric models were considered [43]. It was assumed that the source region is a sphere of radius R around the origin, and that there are no morphogens in the system at $t = 0$. In this case, the concentration profiles are described by [43, 44]

$$\frac{\partial C(r,\,t)}{\partial t} = D\left[\frac{\partial^2 C(r,\,t)}{\partial r^2} + \frac{(d-1)}{r}\frac{\partial C(r,\,t)}{\partial r}\right] - kC(r,\,t). \tag{28}$$

for a d-dimensional system. Here D is the diffusion constant, Q is the production rate at the boundary of the source region, k is the linear degradation rate and $r \geqslant R$. The boundary conditions can be written as [43, 44]

$$-D\frac{\partial C}{\partial r}(R,\,t) = Q. \tag{29}$$

It was also assumed that, far away from the production region, the concentration of the signaling molecules disappears, $C(r \to \infty,\,t) = 0$. At large times, the concentration profiles approach the stationary state, which is given by [44]

$$C_{s,d}(r) = \frac{Q}{\sqrt{Dk}}\frac{K_{d/2-1}(r\sqrt{d}/\lambda)}{K_{d/2}(R\sqrt{d}/\lambda)}\left(\frac{r}{R}\right)^{1-d/2}, \tag{30}$$

where $K_m(y)$ is the mth order modified Bessel function of the second kind and $\lambda = \sqrt{dD/k}$ is the characteristic decay length of the concentration profile in d dimensions. The application of the local relaxation functions provided the explicit expression for the times to reach the stationary state [43, 44],

$$\tau_d(r) = \frac{1}{k} - \frac{(R\sqrt{d}/\lambda)}{2D}\frac{K_{d/2+1}(R\sqrt{d}/\lambda)}{K_{d/2}(R\sqrt{d}/\lambda)} + \frac{(r\sqrt{d}/\lambda)}{2D}\frac{K_{d/2}(r\sqrt{d}/\lambda)}{K_{d/2-1}(r\sqrt{d}/\lambda)}. \tag{31}$$

For two-dimensional systems ($d = 2$), from equations (30) and (31) one could derive the concentration profile [44],

$$C_{s,d=2}(r) = \frac{Q}{\sqrt{Dk}}\frac{K_0(r\sqrt{2}/\lambda)}{K_1(R\sqrt{2}/\lambda)}, \tag{32}$$

and the LAT,

$$\tau_{d=2}(r) = \frac{(r\sqrt{2}/\lambda)}{2k}\frac{K_1(r\sqrt{2}/\lambda)}{K_0(r\sqrt{2}/\lambda)} - \frac{(R\sqrt{2}/\lambda)}{2k}\frac{K_0(R\sqrt{2}/\lambda)}{K_1(R\sqrt{2}/\lambda)}. \tag{33}$$

In the case of $d = 3$, it was shown that [43]

$$C_{s,d=3}(r) = \frac{QR^2 \exp[(R - r)\sqrt{3}/\lambda]}{rD(1 + R\sqrt{3}/\lambda)}, \tag{34}$$

and

$$\tau_{d=3}(r) = \frac{(r - R)\sqrt{3}/\lambda}{2k} + \frac{R\sqrt{3}/\lambda}{2k(1 + R\sqrt{3}/\lambda)}. \tag{35}$$

The analysis of the dynamics of the formation of morphogen gradients in two and three dimensions led to some unexpected results [43]. It was found that, in contrast to one-dimensional systems, there are multiple time scales for approaching the stationary concentration profiles near the production region ($r \simeq R$). It was suggested then that the dimensionality is an important factor in the morphogen gradients' development in multi-dimensional systems, although the mechanisms of this phenomenon were not clarified [43].

These surprising observations were fully explained only when more general multi-dimensional discrete-state stochastic models were introduced [60]. The d-dimensional system with the production at the origin, as shown in figure 6, was investigated. In this system, each lattice site is characterized by d coordinates, $\vec{\mathbf{n}} = (n_1, n_2, \ldots, n_d)$. The source of the signaling molecules is at the origin, $\vec{\mathbf{n}}_0 = (0, 0, \ldots, 0)$, with the production rate Q (see figure 6). Morphogens can diffuse to the nearest neighboring sites with rate u, and the degradation rates at each site are equal to k (figure 6). To solve the problem, a function $P(n_1, n_2, \ldots, n_d; t)$, defined as the probability density at the cell $\vec{\mathbf{n}} = (n_1, n_2, \ldots, n_d)$ at time t, was analyzed at all times using the following master equations [60],

$$\frac{\mathrm{d}P(n_1, n_2, \ldots, n_d; t)}{\mathrm{d}t} = u\sum_{nn} P(n_1, n_2, \ldots, n_d; t) - (2ud + k)P(n_1, n_2, \ldots, n_d; t), \tag{36}$$

where $\sum_{nn}$ corresponds to the summing over all nearest neighbors,

$$\sum_{nn} P(n_1, n_2, \ldots, n_d; t) = P(n_1 - 1, n_2, \ldots, n_d; t) + P(n_1 + 1, n_2, \ldots, n_d; t) + P(n_1, n_2 - 1, \ldots, n_d; t) + P(n_1, n_2 + 1, \ldots, n_d; t) + \ldots. \tag{37}$$

At the origin, the dynamics are slightly different,

$$\frac{\mathrm{d}P(0, 0, \ldots; t)}{\mathrm{d}t} = Q + u\sum_{nn} P(0, 0, \ldots; t) - (2du + k)P(0, 0, \ldots; t). \tag{38}$$

At large times, the system achieves a stationary state with an exponentially decaying signaling concentration profile,

$$P^{(s)}(n_1, n_2, \ldots, n_d) = \frac{2Qx^{|n_1| + |n_2| + \ldots + |n_d|}}{\sqrt{k^2 + 4duk}} = \frac{2Q}{\sqrt{k^2 + 4duk}} \exp\left(\frac{-|n_1| - |n_2| - \ldots - |n_d|}{\lambda}\right), \tag{39}$$

where

$$x = (2du + k - \sqrt{k^2 + 4duk})/(2du), \quad \lambda = -1/\ln x. \tag{40}$$

It was shown also that the dynamics of approaching the stationary state are specified by the LAT [60]

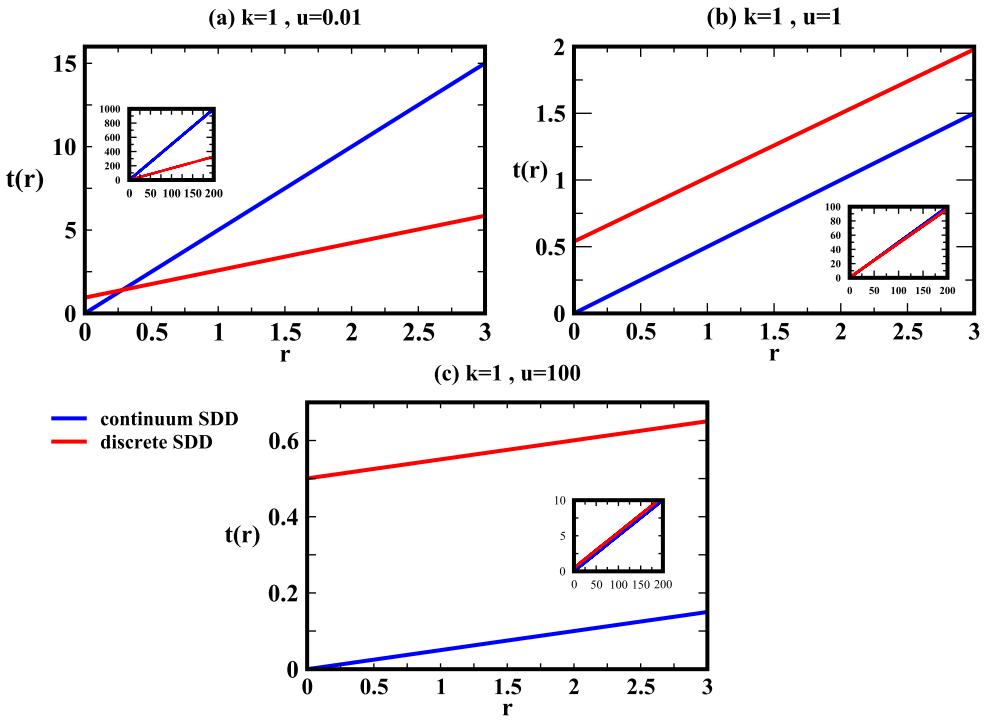

Figure 7. Comparison of the LAT for discrete-state stochastic models and for radially-symmetric continuum models as a function of the distance from the source r in two dimensions. (a) Fast degradation limit, $k = 1$, $u = 0.01$; (b) comparable diffusion and degradation rates, $k = u = 1$; and (c) fast diffusion limit, $k = 1$, $u = 100$. Insets show the same plots for larger length scales. Adapted with permission from [60], copyright 2014 AIP Publishing LLC.

$$t(n_1, n_2, \ldots, n_d) = \frac{(2du + k)}{(k^2 + 4duk)} + \frac{|n_1| + |n_2| + \ldots + |n_d|}{\sqrt{k^2 + 4duk}}. \tag{41}$$

The equivalent expression for the LAT at the distance r from the origin produces [60],

$$\tau(r) = \frac{(2du + k)}{(k^2 + 4duk)} + \left(\frac{\sqrt{d}}{\sqrt{k^2 + 4duk}}\right) r. \tag{42}$$

In the fast degradation limit, $k \gg u$, this equation gives

$$\tau(r) \simeq \frac{1}{k} + \frac{r\sqrt{d}}{k}. \tag{43}$$

In the continuum limit, $u \gg k$, it was found that there is no dependence on the dimensionality [60],

$$\tau(r) \simeq \frac{1}{2k} + \frac{r}{2\sqrt{uk}}. \tag{44}$$

This contrasts with the predictions of the radially-symmetric continuum models [43, 44]. From equation (31) one could obtain for the localized source $R = 0$,

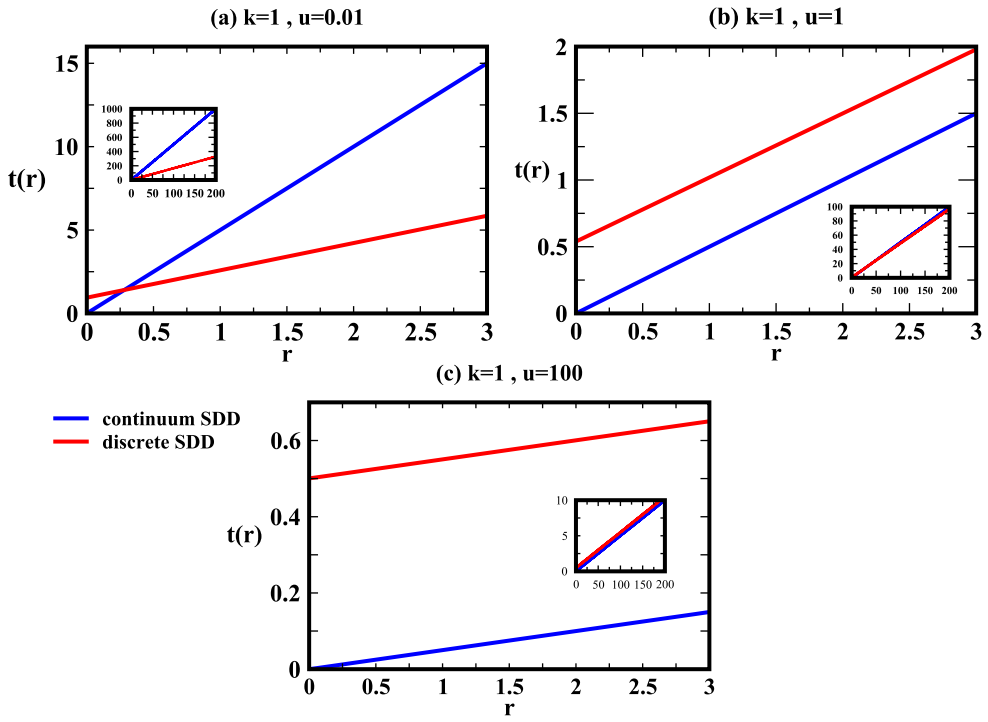

Figure 8. Comparison of the LAT for discrete-state stochastic models and for radially-symmetric continuum models as a function of the distance from the source r in three dimensions. (a) Fast degradation limit, $k = 1$, $u = 0.01$; (b) comparable diffusion and degradation rates, $k = u = 1$; and (c) fast diffusion limit, $k = 1$, $u = 100$. Insets show the same plots for larger length scales. Adapted with permission from [60], copyright 2014 AIP Publishing LLC.

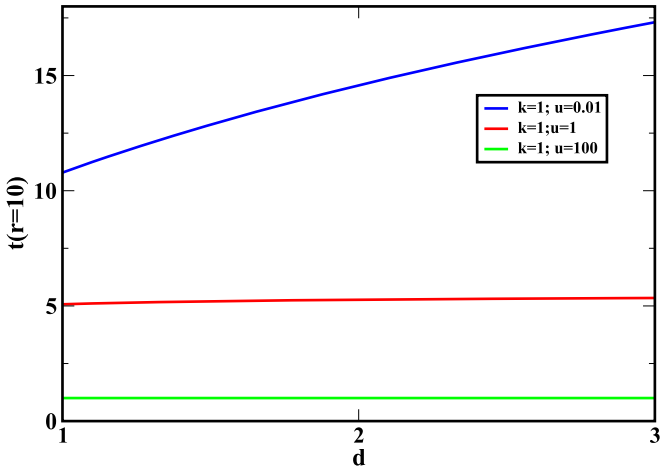

Figure 9. Local accumulation times at $r = 10$ as a function of the spatial dimension. The blue curve corresponds to the fast degradation rates, $k = 1$, $u = 0.01$. The red curve is for the comparable degradation and diffusion rates, $k = u = 1$. The green curve describes the fast diffusion limit, $k = 1$, $u = 100$. Adapted with permission from [60], copyright 2014 AIP Publishing LLC.

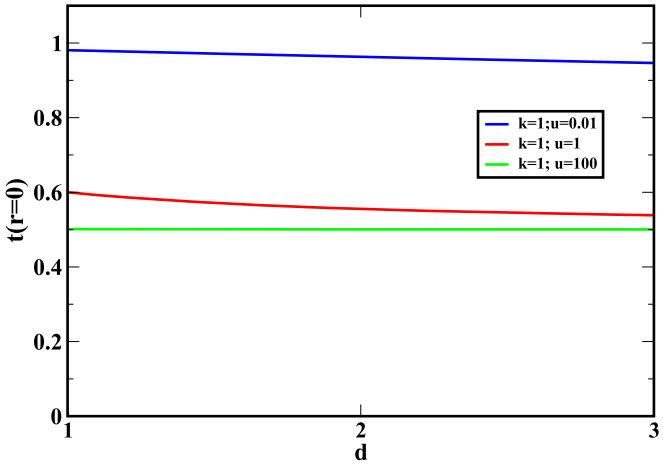

Figure 10. Local accumulation times at $r = 0$ as a function of the spatial dimension. The blue curve corresponds to the fast degradation rates, $k = 1$, $u = 0.01$. The red curve is for the comparable degradation and diffusion rates, $k = u = 1$. The green curve describes the fast diffusion limit, $k = 1$, $u = 100$. Adapted with permission from [60], copyright 2014 AIP Publishing LLC.

$$\tau_d(r) = \frac{1}{k} + \frac{(r\sqrt{d}/\lambda)}{2D}\frac{K_{d/2}(r\sqrt{d}/\lambda)}{K_{d/2-1}(r\sqrt{d}/\lambda)}. \tag{45}$$

To rationalize these deviations between the theoretical predictions, the LAT in two and three dimensions for both approaches have been compared. The results are presented in figures 7 and 8. One can see that the continuum limit of the discrete-state models and radially-symmetric continuum models do not agree with each other, although for large distances ($r \gg 1$) the differences get smaller [60]. It was also noticed that the radially-symmetric models predict that $\tau(r = 0) = 0$, while for the discrete-state case $\tau(r = 0) = 1/2k \neq 0$. But the relaxation times to the stationary profiles can never be zero because originally in the system there are no morphogens. Thus, the radially-symmetric continuum models cannot properly describe the dynamics of the formation of morphogen gradients for $d > 1$ near the production region. The main reason for this is the assumption of the spherically symmetric solutions of the corresponding reaction–diffusion equations at all length scales. The theoretical approach based on the discrete-state stochastic framework does not assume the spherical symmetry and this allows us to correctly describe the dynamics at all scales and in all dimensions [60].

The effect of dimensionality on the dynamics of the formation of morphogen gradients have also been investigated using the discrete-state stochastic models [60]. The results are presented in figures 9 and 10. It was found that the dynamics are determined by the distance from the source and by the relative values of the degradation and diffusion rates. LAT depends on d for fast degradation rates ($k \gg u$), while there is no dependence in the continuum limit ($u \gg k$). The last observation can be simply explained by noting that in the continuum case, the diffusion rate is very fast and the rate-limiting step is the production of morphogens, which is clearly independent of the dimension. Theoretical calculations also show that the LAT for the sites far away from the source ($r \gg 1$) increase with d, while for the sites near the production area ($r \simeq 0$) the trend is reversed: see figures 9 and 10. The following arguments were presented to explain these results [60]. There are two effects by

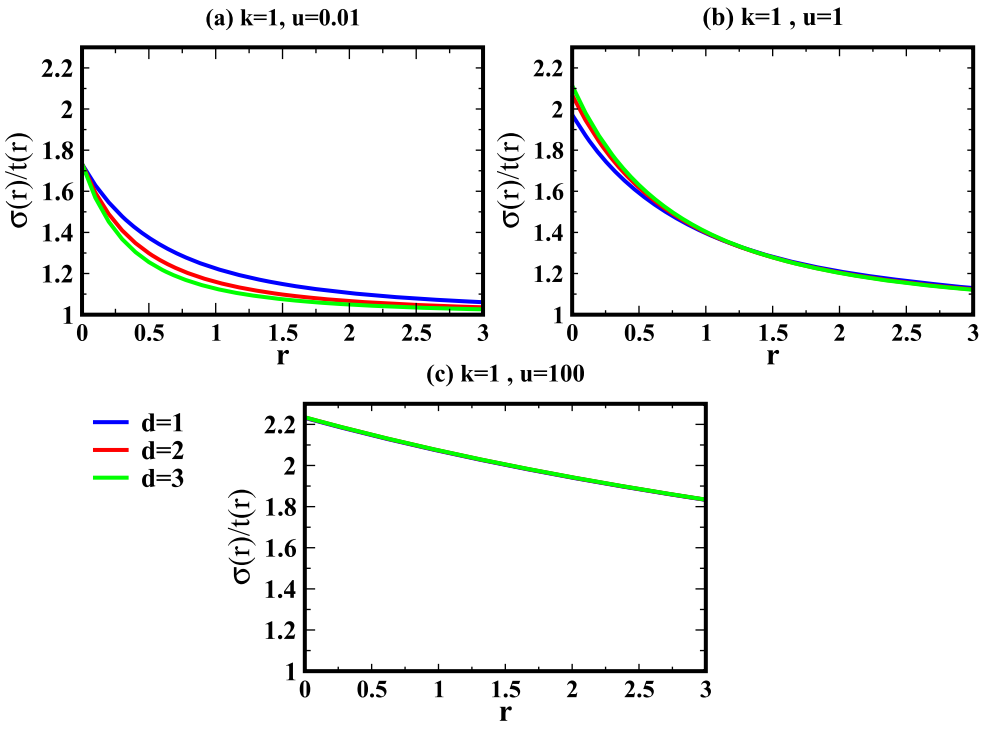

Figure 11. Normalized variance as a function of distance from the source for different dimensions in the discrete-state stochastic models. (a) Fast degradation rates, $k = 1$, $u = 0.01$; (b) comparable degradation and diffusion rates, $k = u = 1$; and (c) fast diffusion rates, $k = 1$, $u = 100$. Adapted with permission from [60], copyright 2014 AIP Publishing LLC.

which the dimension affects the dynamics of the morphogen molecules. Increasing d effectively increases the mobility of the signaling molecules because there are more channels to escape from the given site. At the same time, there are more pathways that connect the source region and any other site on the lattice, and this should increase the relaxation times because there are more long slow trajectories connecting the source and the target cell. The first effect dominates at small distances near the source because there are less pathways to reach the given cell. At the same time, the second effect is more important for large distances.

To investigate in more detail the dynamics of the formation of the signaling profiles, higher moments of the relaxation to the stationary states have been calculated [44, 60]. From this point of view, the LAT is the first moment, $\tau \equiv \langle t \rangle$. Using the discrete-state stochastic method, the variance in the local accumulation times, $\sigma \equiv \sqrt{\langle t^2 \rangle - \langle t \rangle^2}$, was estimated as [60]

$$\sigma(r) = \left[\frac{dr^2 - 2}{(k^2 + 4dk)} + \frac{2r\sqrt{d}\,(2du + k)}{(k^2 + 4duk)^{3/2}} + \frac{5(2du + k)^2}{(k^2 + 4duk)^2} \right]^{1/2}. \tag{46}$$

In the limit of fast degradation rates, $k \gg u$, this expression simplifies into

$$\sigma(r) \simeq \frac{\sqrt{dr^2 + 2r\sqrt{d} + 3}}{k}, \tag{47}$$

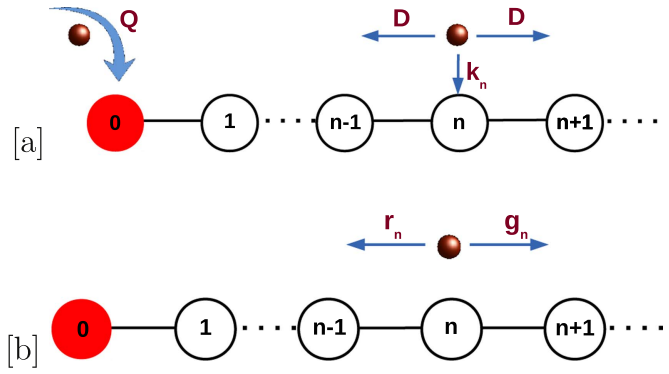

Figure 12. Schematic view of equivalent models for the formation of morphogen gradients. (a) Synthesis-diffusion-degradation model; (b) biased-diffusion model. Adapted with permission from [76], copyright 2015 AIP Publishing LLC.

while in the limit of fast diffusion rates (continuum limit) the variance is

$$\sigma(r) \simeq \frac{\sqrt{5}}{2k} + \frac{r}{2\sqrt{5uk}}. \tag{48}$$

These results suggest that, similar to the LAT, the dependence of the variance of the relaxation times to the stationary profile on the dimension disappears in the continuum limit [60].

The first and second moments of the relaxation times have been further employed in analyzing an important question on how biological systems might control the stochastic noise during the processes of the formation of morphogen gradients [60]. It was argued that the variance normalized by the LAT is a convenient measure of noise, and it is presented in figure 11. Theoretical calculations show that the noise can be reduced by increasing the degradation rate and the dimensionality of the system.

2.5. Nonlinear degradation mechanisms

Several experimental studies suggested that in some systems, the development of the signaling profiles might be associated with more complex nonlinear degradation processes [51, 54–56]. In these situations, the presence of other morphogens can catalyze or inhibit the process of the removal from the medium, and this should affect the dynamics of the formation of morphogen gradients. In this case, the temporal evolution of the concentration profile can be written as [51]

$$\frac{\partial C(x,\,t)}{\partial t} = D\frac{\partial^2 C(x,\,t)}{\partial x^2} - kC(x,\,t)^m, \tag{49}$$

with $m \neq 1$. Using numerical solutions and mathematical bounds, initial studies have shown that the dynamics of approaching the stationary state differ significantly depending on the parameter m [51]. For $m = 0$ and $m = 1$ (linear degradation) LAT are linear functions of the distance from the source, but for $m = 2$, 3 and 4, the scaling changes from linear to quadratic.

The explanations for these surprising observations were presented in the theoretical analysis that proposed viewing the degradation process as an effective driving potential [76]. The degradation creates a gradient by removing molecules from the system, and this is equivalent to the action of the potential given in equation (15) that drives molecules away

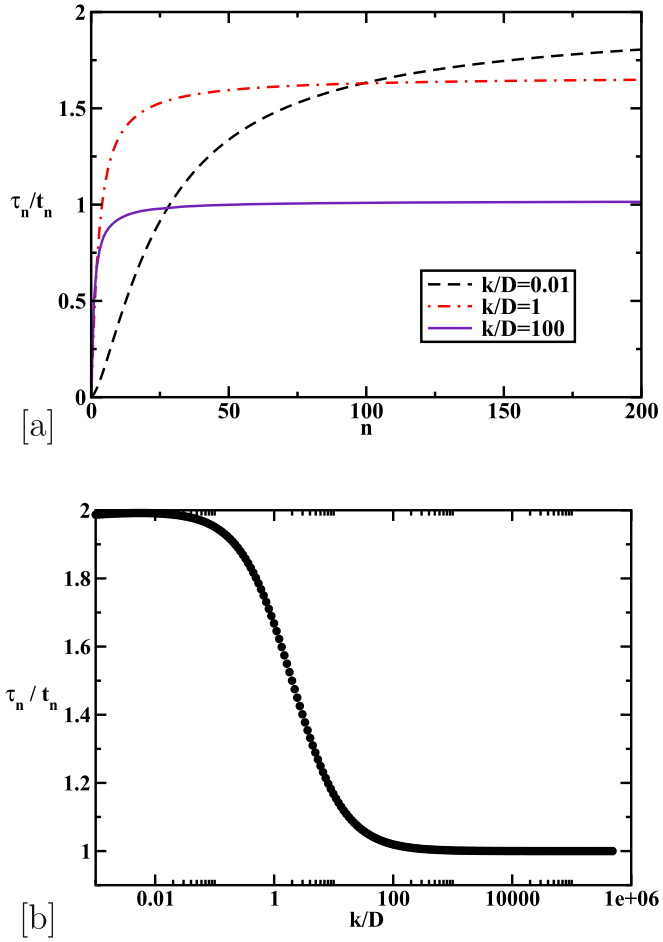

Figure 13. Ratio of calculated mean first passage times for the SDD model and for the equivalent biased-diffusion model. (a) The dependence on the distance from the source; (b) the dependence on the ratio of the degradation rate over the diffusion rate. The distance from the source is set to $n = 10^4$. Adapted with permission from [76], copyright 2015 AIP Publishing LLC.

from the production region. Then the original reaction–diffusion model with the degradation can be approximated as a biased-diffusion model without degradation [76]. This is illustrated in figure 12.

It was assumed that the equivalent biased-diffusion model has L ($L \to \infty$) sites [76]. The morphogens start the motion at $t = 0$ at the origin. The particles can move to the right (left) from site n with the rate $g_n(r_n)$: see figure 12. When the particle reaches site L it is instantaneously moved back to the origin $n = 0$. The model is non-equilibrium, so that there is always a flux in the system in the direction away from the source. In the biased-diffusion model, the probability of finding the molecule at site n at time t is given by a function $\Pi_n(t)$ [76]. The temporal evolution of these probabilities is described by the following master equations [76],

$$\frac{\mathrm{d}\Pi_n(t)}{\mathrm{d}t} = r_{n+1}\Pi_{n+1}(t) + g_{n-1}\Pi_{n-1}(t) - (r_n + g_n)\Pi_n(t), \tag{50}$$

for $0 < n < L$, while for $n = 0$ and $n = L$, we have

$$\frac{\mathrm{d}\Pi_0(t)}{\mathrm{d}t} = J + r_1\Pi_1(t) - g_0\Pi_0(t), \tag{51}$$

$$\frac{\mathrm{d}\Pi_L(t)}{\mathrm{d}t} = g_{L-1}\Pi_{L-1}(t) - r_L\Pi_L(t) - J, \tag{52}$$

where J is the flux from the site L back to the origin $n = 0$. When the system achieves the stationary-state behavior, the flux through every site is equal to J.

Comparing the SDD model and the equivalent biased-diffusion model, it should be clear that the mapping between them is not exact [76]. It can be seen by noting that in the biased-diffusion model there is always a conservation of the probability, while in the SDD model the conservation is only achieved at the stationary-state limit. The relations between the parameters of both models can be made quantitative by using the following arguments. The diffusion rates g_n and r_n are related to each other via the effective potential, as can be shown using the detailed balance-like arguments [76, 82],

$$\frac{g_n}{r_{n+1}} = \exp\left(\frac{U_n^{\mathrm{eff}} - U_{n+1}^{\mathrm{eff}}}{k_{\mathrm{B}}T}\right). \tag{53}$$

The physical meaning of this expression is that the stronger the potential, the faster the motion in the positive direction, $g_n > r_{n+1}$. But to obtain the explicit formulas for the transition rates, a second condition is needed [76],

$$g_n + r_n = 2D + kC^{m-1}. \tag{54}$$

This implies that the residence of each molecule at site n is identical in both models. Together, equations (53) and (54) uniquely define the transition rates in the biased diffusion model via parameters of the SDD model [76].

For linear degradation ($m = 1$) this approach leads to the following transition rates in the equivalent biased-diffusion model [76],

$$g_n = g = \frac{2D + k}{x + 1}, \quad r_n = r = x\frac{2D + k}{x + 1}, \tag{55}$$

with $x = (2D + k - \sqrt{k^2 + 4kD})/2D$. The results for the mean first-passage times from both models are given in figure 13. We conclude that the approximate mapping works quite well everywhere, but especially for large degradation rates.

Extending this method to nonlinear degradation processes indicates that for $m \geqslant 2$ the steady-state profile is given by [76],

$$P_n^{(s)} \simeq \frac{1}{(1 + n/\lambda)^{\frac{2}{m-1}}}, \tag{56}$$

where the parameter λ is defined as

$$\lambda = \frac{1}{m - 1}\left[\frac{(2D)^m(m + 1)}{kQ^{m-1}}\right]^{\frac{1}{m+1}}. \tag{57}$$

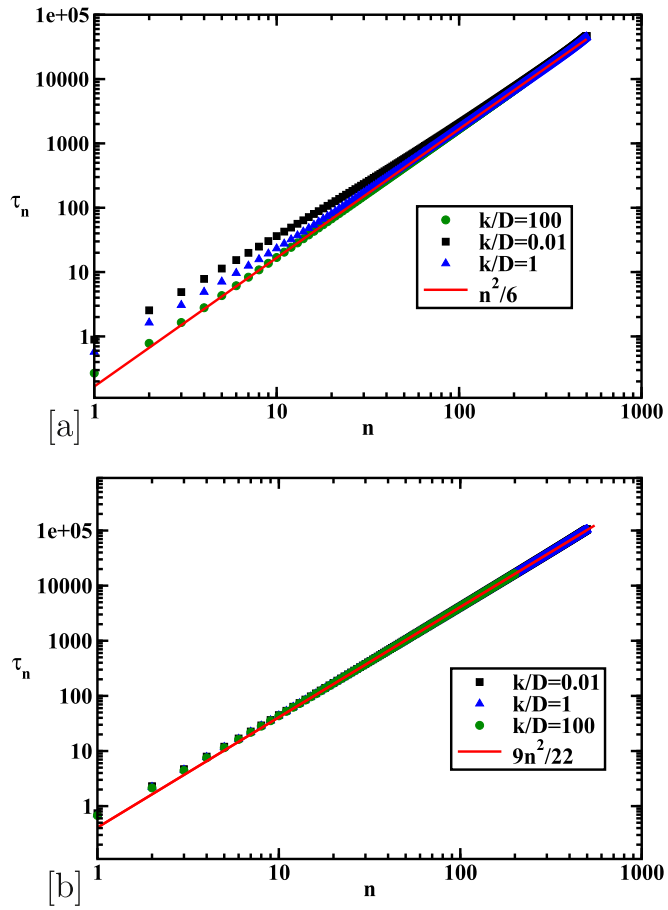

Figure 14. Theoretically calculated mean first-passage times as a function of the distance from the source for different degrees of nonlinearity for the biased-diffusion model. (a) $m = 2$; (b) $m = 10$. Adapted with permission from [76], Copyright 2014 AIP Publishing LLC.

This concentration profile corresponds to the logarithmic potential,

$$\frac{U_n^{\text{eff}}}{k_B T} \simeq -\frac{2}{m-1}\ln(1+n/\lambda). \tag{58}$$

It can be shown that the mean first-passage times for the equivalent biased-diffusion model at large distances from the source are equal to [76]

$$\tau_n \simeq \frac{(m-1)}{(m+1)}\frac{n^2}{2D}. \tag{59}$$

This is an important result since it predicts a quadratic scaling for the relaxation times with the nonlinear degradation, as illustrated also in figure 14.

It is also interesting to note that the approach to the stationary state in nonlinear degradation systems takes place in a self-similar manner for $m > 1$ in one and two dimensions, and for $1 < m < 3$ in three dimensions [84–86]. These results have been obtained using the continuum analysis of the initial boundary value problem. It provided additional

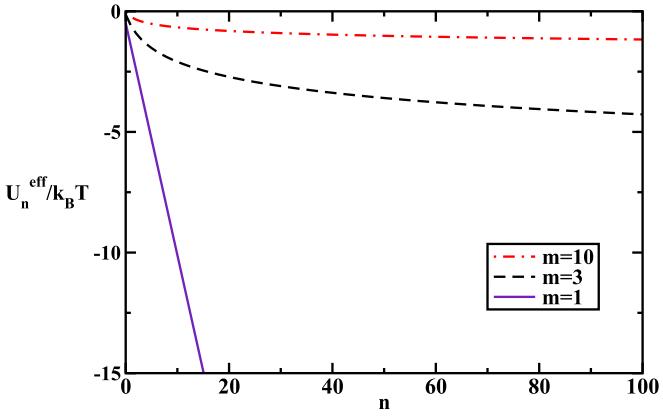

Figure 15. Effective potentials due to degradation. Linear degradation corresponds to $m = 1$, while $m = 3$ and $m = 10$ describe non-linear degradation processes. Adapted with permission from [76], copyright 2015 AIP Publishing LLC.

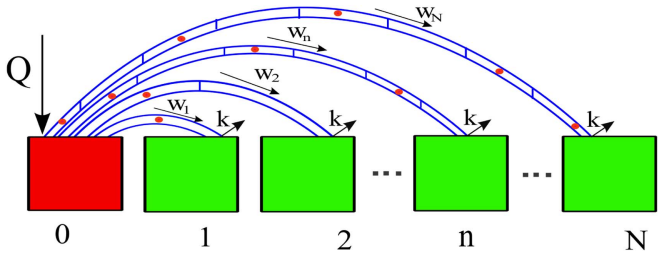

Figure 16. A simplified view of the direct-delivery mechanism of the signaling molecules via the utilization of cytonemes. The red cell is the source. The green cells labeled as $n = 1, \ldots, N$ are the target cells. Cytonemes are shown as tubular extensions from the source cell to the target cells. Morphogens are the small red circles inside the cytonemes. Adapted with permission from [77]. Copyright 2016 American Chemical Society.

arguments to explain the quadratic scaling behavior in the local accumulation times for all non-linear degradation models.

Theoretical calculations using the mapping of the SDD model to the equivalent biased-diffusion model clearly show different scaling behaviors depending on the mechanisms of degradation. Linear scaling is observed for $m = 0$ or 1, while quadratic scaling is found for nonlinear degradations with $m \geqslant 2$ [51, 76]. The different dynamic behavior was explained using the concept of the effective potentials due to degradation [57]. Linear degradation corresponds to a strong driving potential, as shown in figure 15. In this case, there is a unique length scale λ across the whole system. This leads to effectively driven diffusion which has the expected linear scaling. The situation is different for the nonlinear degradation processes. The stationary state in this case can be described by power-law concentration profiles, which do not possess unique length scales. As a result, the effective potential (logarithmic) is weak enough so that it cannot destroy the quadratic scaling of the unbiased diffusion. It might only affect the amplitude of the random-walk fluctuations for each signaling molecule.

2.6. Alternative mechanisms: direct delivery of morphogens

Recent experimental advances in studying the development processes in various systems revealed that there is a significant number of experimental observations that cannot be explained by reaction–diffusion mechanisms [11, 47, 64, 65, 69]. In embryo systems with complex internal structures, simple free diffusion might not always be very efficient in establishing the morphogen gradient [11, 64]. These observations stimulated new ideas on how the genetic information can be transferred in such systems. An alternative direct-delivery mechanism has been proposed [11, 41, 63, 66]. It was suggested that the signaling molecules can be transported to target cells utilizing cellular tubes, which are called cytonemes [11, 41, 63, 66, 69]. Cytonemes are dynamic cellular extensions where cells can extend and retract very quickly with the help of actin filaments. Their length varies from 1–100 μm with a diameter of less than 100 nm. Cytonemes have been recently observed in several biological systems, but their cellular functions were unclear [63–65, 68–71, 74]. It was proposed that morphogens can be transported by myosin motor proteins along the actin filaments inside the cytonemes directly from the source cells to the target cells, as shown schematically in figure 16 [11, 68, 69]. The direct-delivery mechanism thus avoids the problems where a geometrically complex environment prevents the free diffusion forming the signaling profiles.

2.7. Transport through cytonemes

Recently, a first quantitative physical–chemical method to describe the direct delivery via cytonemes has been introduced [77]. It is based on a discrete-state stochastic analysis of the model presented in figure 16. The model assumes that there are $N + 1$ embryo cells in the system (shown as squares in figure 16). One of them (red square, $n = 0$) is a special source cell where the signaling molecules are produced with a rate Q. The source cell also generates N cytonemes that extend and attach to each of the target cells (green squares in figure 16). It is assumed that the cytonemes are already established at the beginning of the process and they are stable until the morphogen gradient is fully established. Signaling molecules (shown as small red circles in figure 16) are transported to the nth target cell from the source cell with a rate w_n ($n = 1, 2, \ldots, N$). When they reach their target cells, morphogens can be degraded with a rate k. This is the minimal model that takes into account the most relevant processes, such as the direct delivery via cytonemes and the degradation of morphogens.

This model can be solved by analyzing the single-molecule probability density function $P_n(t)$ of finding the morphogen at site n at time t. The temporal evolution of this probability function follows the set of master equations [77]

$$\frac{\mathrm{d}P_0(t)}{\mathrm{d}t} = Q - \sum_{n=1}^{N} w_n P_0(t), \tag{60}$$

for $n = 0$, and

$$\frac{\mathrm{d}P_n(t)}{\mathrm{d}t} = w_n P_0(t) - kP_n(t) \tag{61}$$

for $n > 0$. Assuming that initially there were no morphogens in the system, $P_n(t = 0) = 0$ for all n, these master equations can be solved exactly at all times, which leads to

$$P_0(t) = \frac{Q}{\eta}[1 - \mathrm{e}^{-\eta t}]; \tag{62}$$

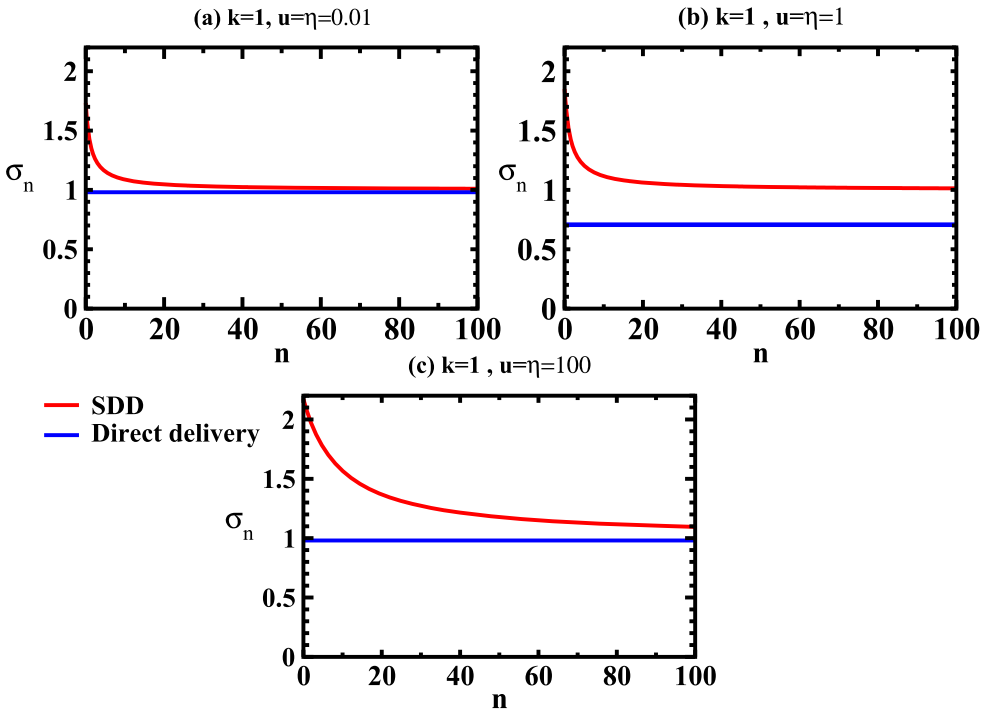

Figure 17. Comparison of normalized variances as a function of the distance from the source for reaction–diffusion and direct-delivery mechanisms. The red lines correspond to the SDD model with a diffusion rate u. The blue lines describe the direct delivery via cytonemes with the total transportation rate η. Adapted with permission from [77]. Copyright 2016 American Chemical Society.

$$P_n(t) = \left[\frac{Qw_n}{\eta(\eta - k)}\right] e^{-\eta t} - \left[\frac{Qw_n}{k(\eta - k)}\right] e^{-kt} + \frac{Qw_n}{\eta k}, \tag{63}$$

where $\eta = \sum_{n=1}^{N} w_n$ is defined as a total production rate from the source cell to all target cells. These results imply that the concentration of signaling molecules at each cell is an exponentially decaying function of the time. It can be viewed as a result of balancing between two opposing processes: the direct delivery with rate η and the removal with rate k. In the stationary-state limit, $(t \to \infty)$, the density profiles reduce to,

$$P_n^{(s)} = \frac{Q}{k\eta} w_n, \quad P_0^{(s)} = \frac{Q}{\eta}. \tag{64}$$

The dynamics of approaching the stationary state can be understood from analyzing a local relaxation function, defined as $R_n(t) \equiv \frac{P_n(t) - P_n^{(s)}}{P_n(0) - P_n^{(s)}}$ [34]. Simple calculations yield the following expressions for the local accumulation times [77],

$$\langle \tau_n \rangle = \frac{1}{k} + \frac{1}{\eta}, \quad \langle \tau_0 \rangle = \frac{1}{\eta}. \tag{65}$$

The model predicts that there is no dependence on the target cell position, n, in contrast to reaction–diffusion mechanisms of the formation of morphogen gradients. The relaxation

dynamics to the stationary concentration profiles are identical for all target cells. The main reason for this is that the processes at all target cells are independent from each other, and the stationary state at each of them cannot be established until the steady-state behavior is observed in the source cell [77]. This can only happen simultaneously in all cells in the system (see figure 16).

Local relaxation functions have also been applied to obtain the second moment of LAT, which allowed us to evaluate the robustness of the direct-delivery mechanism [77]. It was shown that

$$\langle \tau_n^2 \rangle = \frac{2(\eta^2 + k\eta + k^2)}{k^2\eta^2}, \quad \langle \tau_0^2 \rangle = \frac{2}{\eta^2}, \tag{66}$$

which are again independent of the position of the target cell, n. The normalized variance was then computed to be [77],

$$\sigma_n = \left[\frac{\eta^2 + k^2}{\eta^2 + 2k\eta + k^2}\right]^{1/2}, \quad \sigma_0 = 1. \tag{67}$$

The normalized variances for the direct-delivery mechanisms are compared with the corresponding predictions from the reaction–diffusion processes in figure 17. One can see that σ_n is always less for the direct-delivery transport. This means that moving the signaling molecules through the cytonemes is a more robust mechanism of the formation of morphogen gradients because it is affected less by the stochastic noise [77]. In the reaction–diffusion mechanism, the signaling molecules can fluctuate spatially between different cells due to diffusion, but this option is not available for the direct-delivery mechanism. So the advantage of using the transport via cytonemes in creating signaling profiles is not only in overcoming the geometric constraints but also in reducing the influence of the stochastic noise [77].

To better understand how the direct-delivery process works, a more microscopic description of the transportation rates w_n was utilized for calculating the dynamic properties of the system [77]. In the first approach, it was suggested to use the fact that motor proteins drive the morphogens along the cytonemes. It was assumed that the rates are related to the free energy difference of moving the signaling molecule from the source cell to the target cell [77],

$$w_n = \exp\left[-\frac{\Delta G(n)}{k_B T}\right], \tag{68}$$

where $\Delta G(n)$ is the energy required to displace the morphogen to the target cell n. One can assume that the length of the cytoneme to the target cell n, L_n is proportional to n, i.e. $L_n = An$, and the motor proteins spend energy ε (in units of $k_B T$) by moving every signaling molecule a distance l. Then the free energy difference can be written as

$$\Delta G(n) = \frac{L_n \varepsilon k_B T}{l} = \frac{An\varepsilon k_B T}{l} = \frac{nk_B T}{a}, \tag{69}$$

where $a = l/A\varepsilon$. The explicit expression for the transportation rate is given by $w_n = \exp\left[-\frac{n}{a}\right]$. This finally leads to the following expression for the stationary concentration profile [77],

$$P_n^{(s)} = \frac{Q}{k\eta}\exp\left[-\frac{n}{a}\right], \tag{70}$$

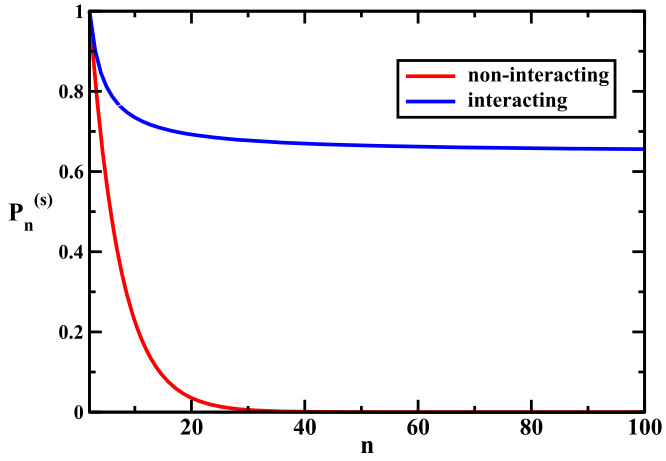

Figure 18. Stationary-state concentration profiles for interacting and non-interacting signaling molecules during the transportation along the cytonemes. Adapted with permission from [77]. Copyright 2016 American Chemical Society.

where the total transportation rate η is equal to

$$\eta = \sum_{n=1}^{N} \exp\left[-\frac{n}{a}\right] = \frac{\exp\left[-\frac{1}{a}\right] - \exp\left[-\frac{(1+N)}{a}\right]}{1 - \exp\left[-\frac{1}{a}\right]}. \tag{71}$$

This model predicts the exponential decaying morphogen gradient (see equation (70)), which is similar to the predictions from the reaction–diffusion models [7–10]. However, the difference is that the decay length in the direct-delivery mechanism, specified by parameter a, is larger for more efficient motor proteins that spend less energy in driving the morphogens along the cytonemes. In the reaction–diffusion mechanism, the decay length is controlled by the ratio of diffusion and degradation rates [34, 57]. Thus the energy dissipation in the transportation of the signaling molecules through the cytonemes is important for the direct-delivery mechanism [77].

Because cytonemes are narrow cylindrical tubes, the transport of the signaling molecules can be viewed as effectively one-dimensional, and this suggests that intermolecular interactions, e.g. due to exclusion, might affect the dynamics [77]. This possibility was investigated using the concept of totally asymmetric exclusion processes (TASEP) [77]. TASEPs are nonequilibrium multi-particle models that were successfully utilized for uncovering the mechanisms of many complex biological processes [73]. It was proposed that each cytoneme can be viewed as a one-dimensional lattice on which morphogens move in the direction of the target cell. The problem of describing the dynamics of the formation of morphogen gradients in such a system is identical to a set of open-boundary TASEP segments coupled at the source cell. Stationary-state fluxes for TASEP on finite lattice segments with an entrance rate α and an exit rate β are well known [72],

$$J(\alpha, \beta; n) = \frac{S_{n-1}(1/\beta) - S_{n-1}(1/\alpha)}{S_n(1/\beta) - S_n(1/\alpha)}, \tag{72}$$

where

$$S_n(y) = \sum_{i=0}^{n-1} \frac{(n - \mathrm{i})(n + \mathrm{i} - 1)!}{n!i!} y^{n-\mathrm{i}+1}. \tag{73}$$

For the model presented in figure 16, the entrance and exit rates on each cytoneme are given by [77],

$$\alpha = Q/N, \quad \beta = k. \tag{74}$$

The transition rate from the source cell to the target cell n can be written as

$$w_n = J(Q/N, k; n). \tag{75}$$

The stationary-state profile in this system of interacting morphogens is equal to

$$P_n^{(s)} = \frac{Q}{k\eta} \frac{S_{n-1}(1/k) - S_{n-1}(N/Q)}{S_n(1/k) - S_n(N/Q)}. \tag{76}$$

Figure 18 illustrates the morphogen gradients for this system of interacting signaling molecules. The possibility of interactions between the morphogen molecules has a dramatic effect on the stationary profiles. While at distances not far away from the source the effect is minimal, for larger distances the density profile saturates. But this leveling is not useful for the morphogen gradients because the information can be transferred efficiently only from strongly decaying profiles. It was suggested that these intermolecular interactions might present a problem for the direct-delivery mechanism for very large distances, but experimental tests of these predictions are needed because many other factors might change the outcome [77].

It is also important to note that the transport of morphogen molecules along the cytonemes could be more complex due to the possibility of various super-diffusive or sub-diffusive processes [87–89]. These processes might arise because of dense crowding and a viscoelastic environment of the living cells, and because of the complex intermolecular interactions. All these factors can significantly modify the dynamics of the formation of morphogen gradients under direct-delivery conditions.

3. Concluding remarks and future directions

To conclude, we presented a review of the recent developments in the theoretical understanding of the mechanisms that lead to the formation of biological signaling profiles. The dynamics of the formation of morphogen gradients was analyzed first using the reaction–diffusion framework. This is assumed to be the main mechanism for creating the concentration profiles of signaling molecules that can efficiently transfer the information in embryo systems. We discussed the critical role of the degradation processes, and it was argued that its action is similar to the driving potential that accelerates the dynamics of the formation of morphogen gradients. Several other important aspects of the development of signaling profiles, including the effect of the size of the production region, dimensionality, nonlinearity in the degradation and discreteness of these processes, have been thoroughly analyzed. We also discussed the alternative direct-delivery mechanisms in the establishment of morphogen gradients. The presented theoretical methods are applicable to a broad range of biological development phenomena, as well as for cell signaling and tissue and organ formation processes.

Although many features of the development of signaling profiles are now better understood, there are many puzzling questions and observations in the field. Let us briefly

mention several of them. The production of the morphogens is a time-dependent process with variable rates. But existing theoretical methods mostly assume that these rates are constant. It is not clear how to take into account the temporal effect in the source and what effect it might have on dynamics. Another challenging problem is whether the morphogen gradient needs to reach the stationary state or not in order to properly transfer the information. There are controversial views about the possibility of the pre-steady state decoding as the more efficient mechanism of information transfer [23, 58]. It is important to understand this because it might affect the dynamics and the robustness of the system. Another critical question is related to the fact that embryo cells during the formation of morphogen gradients are not frozen as implicitly assumed in current theoretical models. They are dynamic systems that can grow, shrink, divide and change shape. New theoretical ideas are needed in order to couple the chemical and biophysical processes of the formation of morphogen gradients with mechanical stability and transformations in embryo cells. Finally, it is still unclear how exactly the embryo cells read the information from the signaling profiles. Several ideas were expressed but none of them are fully supported by existing experimental data [47]. It is critically important to combine multiple theoretical, computational and experimental methods to advance our knowledge on the mechanisms of these fundamental biological processes.

Acknowledgments

The work was supported by grants from the Welch Foundation (C-1559), from the NSF (Grant CHE-1360979) and by the Center for Theoretical Biological Physics sponsored by the NSF (Grant PHY-1427654).

References

[1] Martinez-Arias A and Stewart A 2002 *Molecular Principles of Animal Development* (New York: Oxford University Press)
[2] Lodish H, Berk A, Kaiser C A, Krieger M, Scott M P, Bretscher A, Ploegh H and Matsudaira P 2007 *Molecular Cell Biology* 6th edn (New York: Freeman)
[3] Wolpert L 1998 *Principles of Development* (New York: Oxford University Press)
[4] Wolpert L 1969 Positional information and the spatial pattern of cellular differentiation *J. Theor. Biol.* **25** 1
[5] Crick F H 1970 *Nature* **225** 420
[6] Turing A M 1952 *Phil. Trans. R. Soc.* **237** 37
[7] Porcher A and Dostatni N 2010 *Curr. Biol.* **20** R249
[8] Briscoe J and Small S 2015 *Development* **142** 3996
[9] Lander D A 2007 *Cell* **128** 245
[10] Wartlick O, Kicheva A and Gonzales-Gaitan M 2009 *Cold Spring Harb. Perspect. Biol.* **1** a001255
[11] Kornberg T B 2012 *Biophys. J.* **103** 2252
[12] Rogers K W and Schier A F 2011 *Annu. Rev. Cell Dev. Biol.* **27** 377
[13] Kerszberg M and Wolpert L 1998 *J. Theor. Biol.* **191** 103
[14] Tabata T and Takei Y 2004 *Development* **131** 703
[15] Kerszberg M and Wolpert L 2007 *Cell* **130** 205
[16] Gregor T, Wieschaus E F, McGregor A P, Bialek W and Tank D W 2007 *Cell* **130** 141
[17] Cheung D, Miles C, Kreitman M and Ma J 2014 *Development* **141** 124
[18] Zhou S, Lo W C, Suhalim J L, Digman M A, Grattom E, Nie Q and Lander A D 2012 *Curr. Biol.* **22** 668
[19] Yu S R, Burkhardt M, Nowak M, Ries J, Petrasek Z, Scholpp S, Schwille P and Brand M 2009 *Nature* **461** 533

[20] Dessaud E, Yang L L, Hill K, Cox B, Ulloa F, Ribeiro A, Mynett A, Novitch B G and Briscoe J 2007 *Nature* **450** 717
[21] Berezhkovskii A M and Shvartsman S Y 2013 *J. Chem. Phys.* **138** 244105
[22] Mogilner A and Odde D 2011 *Trends Cell Biol.* **21** 692
[23] Bergmann S, Sandler O, Sberro H, Shnider S, Schejter E, Shilo B-Z and Barkai N 2007 *PLoS Biol.* **5** 232
[24] Entchev E V, Schwabedissen A and Gonzales-Gaitan M 2000 *Cell* **103** 981
[25] Müller P, Rogers K W, Jordan B M, Lee J S, Robson D, Ramanathan S and Schier A F 2012 *Science* **336** 721
[26] Spirov A, Fahmy K, Schneider M, Frei E, Noll M and Baumgartner S 2009 *Development* **136** 605
[27] Drocco J A, Grimm O, Tank D W and Wieschaus E 2011 *Biophys. J.* **101** 1807
[28] Little S C, Tkacik G, Kneeland T B, Wieschaus E F and Gregor T 2011 *PLoS Biol.* **9** e1000596
[29] Grimm O, Coppy M and Wieschaus E 2009 *Development* **137** 2253
[30] Lipshitz H D 2009 *Nat. Rev. Mol. Cell Biol.* **10** 509
[31] Dalessi S, Neves A and Bergmann S 2012 *J. Theor. Biol.* **294** 130
[32] Deng J, Wang W, Lu L J and Ma J 2010 *PLoS Biol.* **5** e10275
[33] Drocco J A, Wieschaus E F and Tank D W 2012 *Phys. Biol.* **9** 055004
[34] Berezhkovskii A M, Sample C and Shvartsman S Y 2010 *Biophys. J.* **99** L59
[35] Berezhkovskii A M 2011 *J. Chem. Phys.* **135** 074112
[36] Berezhkovskii A M and Shvartsman S Y 2011 *J. Chem. Phys.* **135** 154115
[37] Berezhkovskii A M, Sample C and Shvartsman S Y 2011 *Phys. Rev.* E **83** 051906
[38] Yuste S B, Abad E and Lindenberg K 2010 *Phys. Rev.* E **82** 061123
[39] Krotov D, Dubuis J O, Gregor T and Bialek W 2014 *Proc. Natl Acad. Sci. USA* **111** 3683
[40] Tufcea D E and Francois P 2015 *Biophys. J.* **109** 1724
[41] Müller P, Rogers K W, Yu S R, Brand M and Schier A F 2013 *Development* **140** 1621
[42] Medioni C, Mowry K and Bess F 2012 *Development* **139** 3263
[43] Gordon P V, Muratov C B and Shvartsman S Y 2013 *J. Chem. Phys.* **138** 104121
[44] Ellery A J, Simpson M J and McCue S W 2013 *J. Chem. Phys.* **139** 017101
[45] Sigaut L, Pearson J E, Colman-Lerner A and Dawson S P 2014 *PLoS Comp. Biol.* **10** e1003629
[46] Kicheva A, Pantazis P, Bollenbach T, Kalaidzidis Y, Bittig T, Jülicher F and Gonzales-Gaitan M 2007 *Science* **315** 521
[47] Richards D M and Saunders T E 2015 *Biophys. J.* **108** 2061
[48] Briscoe J 2009 *EMBO J.* **28** 457
[49] Alaynick W A, Jessell T M and Pfaff S L 2011 *Cell* **146** 178
[50] Fedotov S and Falconer S 2014 *Phys. Rev.* E **89** 012107
[51] Gordon P V, Sample C, Berezhkovskii A M, Muratov C B and Shvartsman S Y 2011 *Proc. Natl Acad. Sci. USA* **108** 6157
[52] Sample C and Shvartsman S Y 2010 *Proc. Natl Acad. Sci. USA* **107** 10092
[53] Castle B T, Howard S A and Odde D J 2011 *Cell Mol. Bioeng.* **4** 116
[54] Eldar A, Rosin D, Shilo B-Z and Barkai N 2003 *Dev. Cell.* **5** 635
[55] Chen Y and Struhl G 1996 *Cell* **87** 553
[56] Incardona J P, Lee J H, Robertson C P, Enga K, Kapur R P and Roelink H 2000 *Proc. Natl Acad. Sci. USA* **97** 12044
[57] Kolomeisky A B 2011 *J. Phys. Chem. Lett.* **2** 1502
[58] Saunders T and Howard M 2009 *Phys. Biol.* **6** 046020
[59] England J L and Cardy J 2005 *Phys. Rev. Lett.* **94** 078101
[60] Teimouri H and Kolomeisky A B 2014 *J. Chem. Phys.* **140** 085102
[61] Tompkins N, Li N, Girabawe C, Heymann M, Ermentrout G B, Epstein I R and Fraden S 2013 *Proc. Natl Acad. Sci.* **111** 4397
[62] Dilao R and Muraro D 2010 *J. Theor. Biol.* **264** 847
[63] Kornberg T B and Roy S 2014 *Trends Cell. Biol.* **24** 370
[64] Roy S and Kornberg T B 2015 *Bioessays* **37** 25
[65] Fairchild C L and Barna M 2014 *Curr. Opin. Genetics Dev.* **27** 67
[66] Rørth P 2014 *Science* **343** 848
[67] Kornberg T B and Roy S 2014 *Development* **141** 729
[68] Sanders T A, Llagostera E and Barna M 2013 *Nature* **497** 628
[69] Gradilla A-C and Guerrero I 2013 *Cell. Tissue Res.* **352** 59
[70] Guerrero I and Kornberg T B 2014 *Semin. Cell Dev. Biol.* **33** 52

[71] Bischoff M, Gradilla A C, Seijo I, Andrés G, Rodríguez-Navas C, González-Méndez L and Guerrero I 2013 *Nat. Cell Biol.* **15** 1269
[72] Derrida B, Evans M R, Hakim V and Pasquier V 1993 *J. Phys.* A **26** 1493
[73] Chou T, Mallick K and Zia R K P 2011 *Rep. Prog. Phys.* **74** 116601
[74] Cohen M, Georgiou M, Stevenson N L, Miodownik M and Baum B 2010 *Dev. Cell* **19** 78
[75] Teimouri H and Kolomeisky A B 2015 *Phys. Biol.* **12** 026006
[76] Bozorgui B, Teimouri H and Kolomeisky A B 2015 *J. Chem. Phys.* **143** 025102
[77] Teimouri H and Kolomeisky A B 2016 *J. Phys. Chem. Lett.* **7** 180
[78] Teimouri H, Bozorgui B and Kolomeisky A B 2016 *J. Phys. Chem.* B **120** 2745
[79] Hecht I, Rappel W-J and Levine H 2009 *Proc. Natl Acad. Sci. USA* **106** 1710
[80] Reingruber J and Holcman D 2014 *Semin. Cell Dev. Biol.* **35** 189
[81] Redner S 2001 *A Guide to First-Passage Processes* (Cambridge: Cambridge University Press)
[82] Van Kampen N G 2001 *Stochastic Processes in Physics and Chemistry* (Amsterdam: Elsevier)
[83] Kicheva A, Bollenbach T, Wartlick O, Jülicher F and Gonzalez-Gaitan M 2012 *Curr. Opin. Genetics Dev.* **22** 527
[84] Muratov C B, Gordon P V and Shvartsman S Y 2011 *Phys. Rev.* E **84** 041916
[85] Gordon P V and Muratov C B 2012 *Netw. Heterogeneous Media* **7** 767
[86] Gordon P V and Muratov C B 2015 *SIAM J. Math. Anal.* **47** 2903
[87] Reverey J F, Jeon J-H, Bao H, Leippe M, Metzler R and Selhuber-Unker C 2015 *Sci. Rep.* **5** 11690
[88] Metzler R, Jeon J-H, Cherstvy A G and Barkai E 2014 *Phys. Chem. Chem. Phys.* **16** 24128
[89] Hofling F and Franosh T 2013 *Rep. Prog. Phys.* **76** 046602